Implementing Badhwar-O'Neill GCR Model for the Analysis of Space Radiation Exposure

Myung-Hee Y. Kim[1]
Patrick M. O'Neill[2]
Tony C. Slaba[3]

[1]Wyle Science, Technology and Engineering, Houston, TX 77058
[2]NASA Johnson Space Center, Houston, TX 77058
[3]NASA Langley Research Center, Hampton, VA 23681

WRMISS-19, Krakow, Poland, September 9-11, 2014

Outline

- GCR Background and Measurements
- BO11 GCR Model
- GCR Model and Transport Code Validation on ISS/STS
- GCR Model and Transport Code Validation on Mars surface
- Recent updates to BO GCR Model: BO13
- Conclusions

Introduction

Discovery and Understanding of the GCR Energy Spectrum in Interplanetary Space throughout the Heliosphere (~100 AU)

- Ionizing radiation in natural ores discovered by Henri Becquerel in 1895
- CR from outer space discovered by Victor Hess in 1912
- Origin of GCR from the exploding stars of our galaxy, especially core-collapse supernovas
- Mainly protons (90%), significant numbers of helium (9%), ions from Li through the Fe-Ni group (the most of remaining 1%), and elements up to Z=92 (0.00003%)
- GCRs accelerate in interstellar space by collisions with moving magnetic fields suggested by Enrico Fermi in 1979
- A power law in energy observed for all GCRs at the higher E > 20 GeV/n → No solar modulation
- Local Interstellar Spectrum (LIS) at the far edge of the heliosphere is constant and isotropic
- GCRs attenuate at the region of sun's magnetic field especially at the lower E < 20 GeV/n → GCR modulation inside the heliosphere

GCR Measurements

- Early Measurements:
  - Ionization chambers since 1920's
  - Balloons and CR detectors throughout 1930's and reached to TOA (100k feet) by 1940
  - Balloon flights at TOA for *p* and *He* energy spectra by 1950
  - Neutron monitors monitoring high energy *p* and *He* around the world since 1950's
  - Balloon and satellite energy spectra from 1950's – 1980's
    - High altitude balloons for *p* and *He* spectra from 50 MeV/n to 50 GeV/n
    - Detector technology: Si barrier coincident hodoscopes, Cerenkov scintillation telescopes, ionization spectrometers, photo multiplier tubes, and nuclear emulsions
    - First satellite measurement of Interplanetary Monitoring Platform (IMP-1) in 1963
  - Pioneer 8 (1967) in route to Jupiter observed anomalous component below ~50 MeV/n
- Modern measurements:
  - Balloon-borne Experiment with Superconducting Spectrometer (BESS) for *p* and *He* observation from 1993-2002
  - Isotope Matter-Antimatter Experiment (IMAX) for improved light ions' spectra in 1992
  - NASA Advanced Composition Explorer (ACE) Cosmic Ray Isotope Spectrometer (CRIS) for daily spectra of low energy (50-500 MeV/n) heavy ions (Z>2) since 1997
  - NASA High Energy Astrophysics Observatory -3 (HEAO-3) satellite launched 1979 for the most precise data available about the isotopic composition of GCR's above 2 GeV/n (LIS spectrum defined)
  - Alpha Magnetic Spectrometer (AMS-2) mounted on ISS since 2011 – new measurements for GCR's

BO11 GCR Model

- GCR Model with practical features of GCR measurements for the certification of micro-electronic systems and the analysis of radiation health risks to astronauts in space missions.
  - Solar Modulation

    Level is derived from the mean International Sunspot numbers after taking account for
    - Time delays due to the response of heliosphere to solar sunspot activity
    - Time delays due to the rigidity of the different GCR elements
    - Global effects due to the polarity of the heliospheric magnetic field (gradient and curvature drift)
  - The overall solar modulation effect is essentially the same regardless of the state of the heliosphere.
    - A single, simple, empirical modulation parameter (Φ) represents the solar modulation, which affects the shape of the GCR spectra and the overall magnitude of spectrum
  - Particle Transport in the Heliosphere

    Fokker-Planck equation due to diffusion, convection, and adiabatic deceleration is solved empirically to account for dynamics and anti-symmetrical features of the heliosphere
    - Radially dependent diffusion coefficient from the magnetic disturbances at the constant solar wind speed
    - Polarity dependence due to gradient and curvature by Plateau and Peaked due to Coronal Mass Ejections (CME's)

O'Neill, PM and CC Foster, Badhwar-O'Neill 2011 Galactic Cosmic Ray Flux Model Description, NASA/TP-2013-217376.

Solar Modulation from Sunspot Number

For Z=1

$$\Phi = 420 + 5.4 \times ISS$$

For Z>1

$$\Phi_{Peaked} = 420 + 5.4 \times ISS$$

$$\Phi_{Plateau} = 420 + 2.8 \times ISS$$

Peaked period during B^- magnetic field:

immediate response to new solar cycle with minimal delay

Plateau period during B^+ magnetic field:

a rapid GCR rise followed by a delayed decline

Solar Modulation Parameter (Φ)

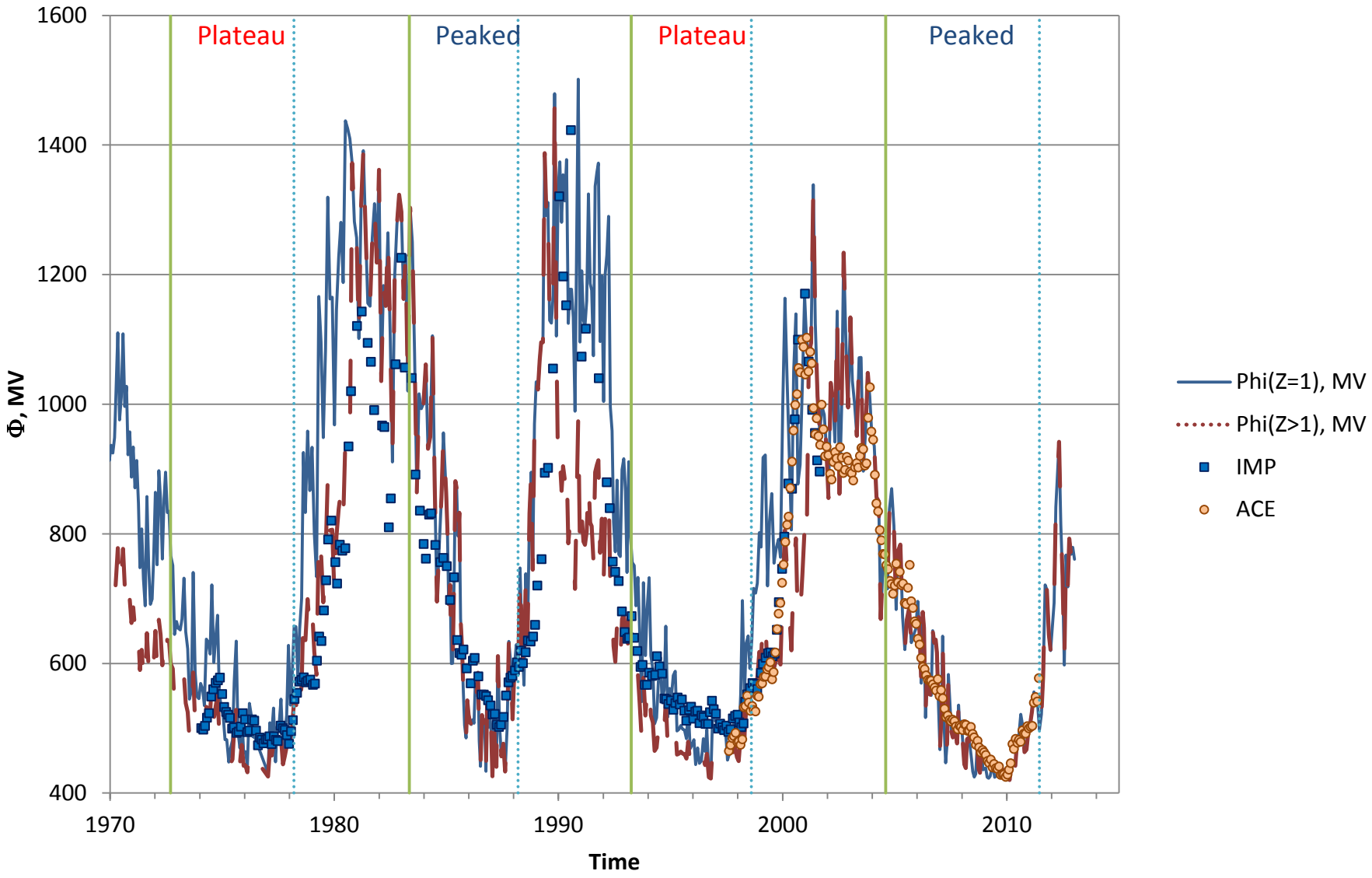

Time Delay and Impact on the Heliosphere Regarding Modulation of Protons

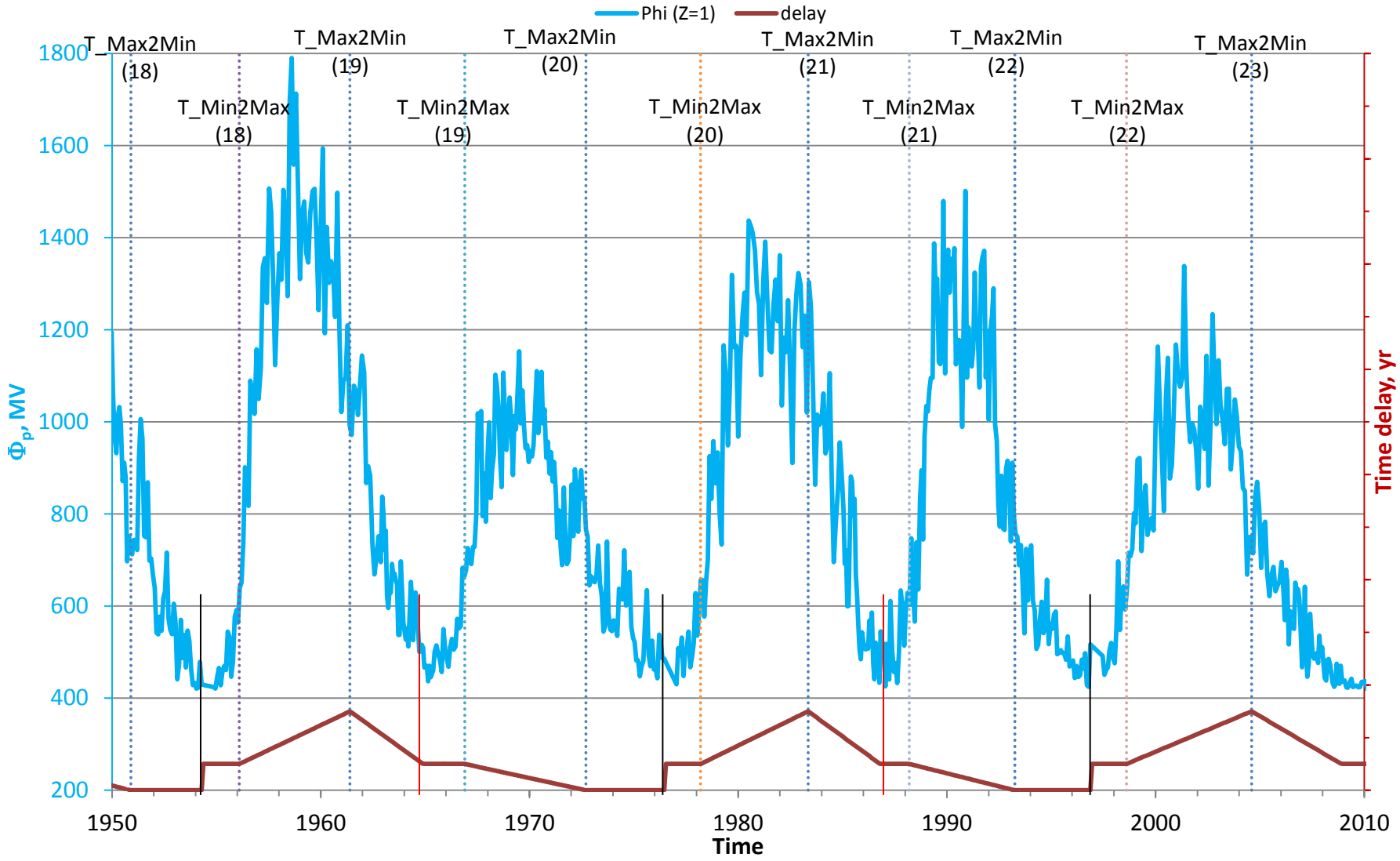

Comparison of GCR Fe Nuclei at 1 AU

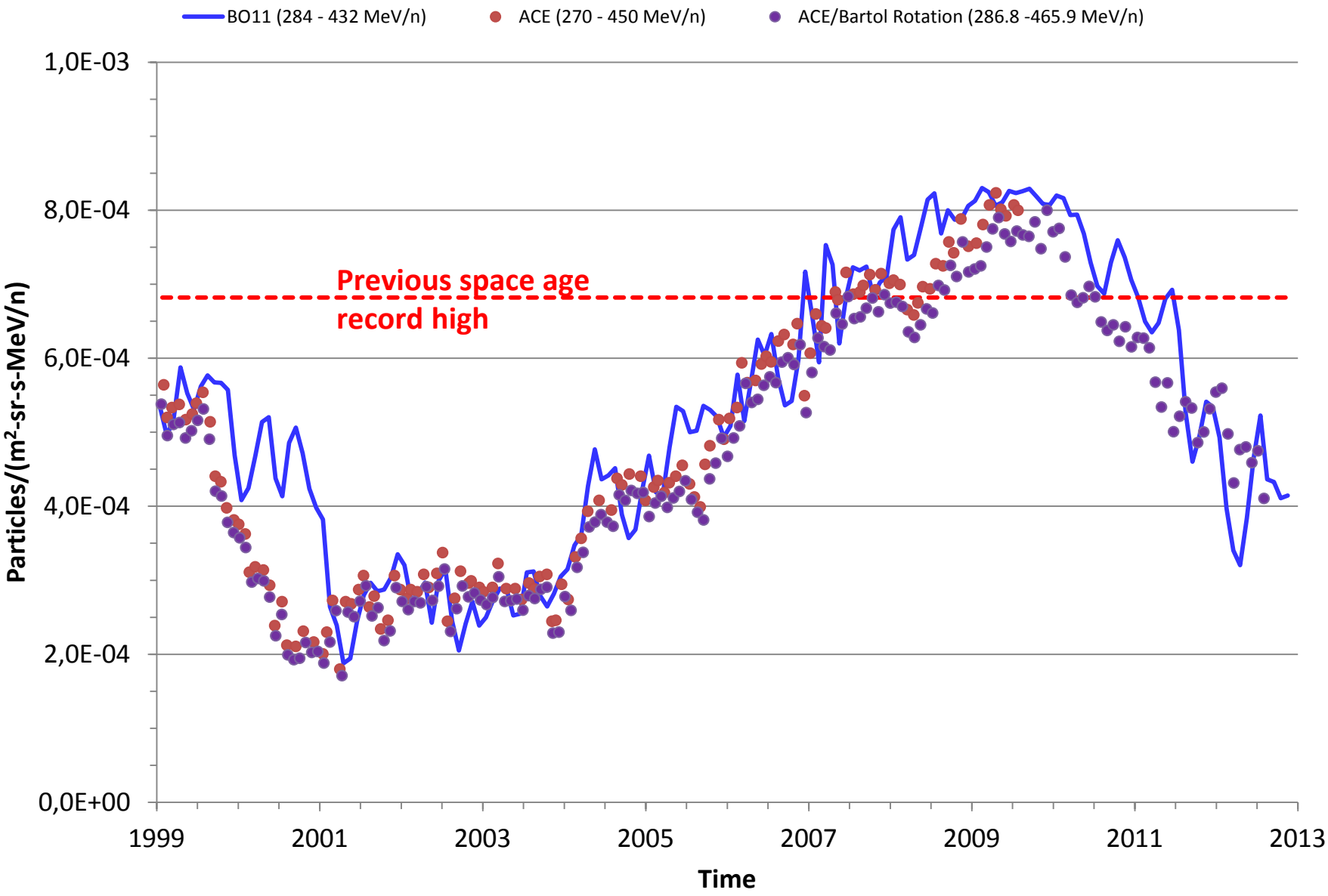

Model Parameters at LEO

year	BO96	DLR		BO11	
	Φ(Climax(t-3))	Φ for p albedo	Annual SSN	$\Phi(ACE)_p$	$\Phi(ACE)_{He}$
1997	514	477	22	491	456
1998	547	560	64	644	536
1999	660	727	93	819	627
2000	1225	944	120	1005	723
2001	1221	1092	111	1062	1022
2002	1226	1057	104	1021	1021
2003	1291	1022	64	1009	1009
2004	1111	852	40	808	808
2005	808	720	30	684	684
2006	675	618	15	605	605
2007	514	546	8	510	510
2008	480	487	3	452	452
2009	397	440	3	429	429
2010	451	458	17	467	467
2011	603	603	56	581	581
2012	677	738	57	769	769

Parameters for GCR Model		
BO96	**DLR**	**BO11**
GCR at 1 AU		
Φ(Climax NM)	Oulu NM and Sunspot number	Φ(SS)
At LEO: 51.6°X400 km		
- GCR transmission factor at 51.6 - Earth shadow effect : 400 km - Neutron Albedo: 400 km & sunspot number - Proton Albedo: Φ		
No trapped proton (dumF10.7=70)		
No pion	Pion correction	

- Pions, Muons, Gamma-rays, and Electrons are low LET with much lower QF or RBE compared to GCR ions
  - Pion/EM cascade included using an empirical correction factor, any material scaled to aluminum with average mass [Cucinotta et al., 2013], and QF=1.2 assumed

Model Comparison to TEPC Measurements

GCR model	STS-92								mrad/d TEPC-GCR	mrem/d TEPC-GCR	177 nm	Φ_p	Φ_{He}
	Date	**Days**	**Incli.**	**Alt , km**	**SS Num**	**Φ, MV**	**F10.7**	**Fbar**					
	10/11/2000	12.90	51.6	388	140.0	1187	158.0	158.0	10.29	43.6			
BO11				**328**	**99.4**		**149.9**		**8.79**	**38.54**	0-sphere	**923.61**	**681.1**
$BO10_{adj}$	$\Phi_{ACE/adj}$			328	**99.4**	**816.58**	149.9		**7.81**	**30.43**		849.7	725.1
DLR	Φ_{ACE}			328	**99.4**	**816.58**	149.9		**7.39**	**29.54**			
	STS-81								mrad/d TEPC-GCR	mrem/d TEPC-GCR	184 statute miles	Φ_p	Φ_{He}
	Date	**Days**	**Incli.**	**Alt , km**	**SS Num**	**Φ, MV**	**F10.7**	**Fbar**					
	1/12/1997	10.20	51.6	354	4.3	553	72.4	73.0	14.7	47.9			
BO11				**296**	**5.7**		**64.5**		**12.24**	**50.79**	0-sphere	**509.4**	**466.4**
$BO10_{adj}$	$\Phi_{ACE/adj}$			296	**5.7**	**491.57**	64.5		**11.68**	**43.99**		412.7	449.7
DLR	Φ_{ACE}			296	**5.7**	**491.57**	64.5		**11.62**	**45.78**			
	STS-89								mrad/d TEPC-GCR	mrem/d TEPC-GCR	160 nm	Φ_p	Φ_{He}
	Date	**Days**	**Incli.**	**Alt, km**	**SS Num**	**Φ, MV**	**F10.7**	**Fbar**					
	1/22/1998	8.82	51.6	296	50.3	493	94.6	92.4	17.6	56.1			
BO11					**31.9**		**81.4**		**12.31**	**51.03**	0-sphere	**503.5**	**463.3**
$BO10_{adj}$	$\Phi_{ACE/}$			296	**31.9**	**515.21**	81.4		**11.18**	**42.35**		453.2	469.7
DLR	Φ_{ACE}			296	**31.9**	**515.21**	81.4		**11.53**	**45.44**			
BO96	$\Phi_{ClimaxNM}$					**501.13**			**13.55**	**46.68**			

STS-89 Mission for TEPC Experiment

	STS-89								mrad/d	mrem/d			
	Date	Days	Incli.	Alt (km)	SS Num	Φ, MV	F10.7	Fbar	TEPC-GCR	TEPC-GCR	160 nm	Φ_p	Φ_{He}
	1/22/1998	8.82	51.6	296	50.3	493	94.6	92.4	17.6	56.1			
BO11				**296**	**31.9**		**81.4**		**12.31**	**51.03**	**0 sphere**	**503.5**	**463.3**
BO10_a	$\Phi_{ACE/adj}$			296	**31.9**	**515.21**	81.4		**11.18**	**42.35**		453.2	469.7
DLR	Φ_{ACE}			296	**31.9**	**515.21**	81.4		**11.53**	**45.44**			
BO96	$\Phi_{ClimaxNM}$					**501.13**			**13.55**	**46.68**			
	1/22/1998	8.82	51.6	296	50.3	493	94.6	92.4	16.7	44.5			
BO11				**296**	**31.9**		**81.4**		**14.68**	**44.82**	**Al 5" sphere**	**503.5**	**463.3**
BO10_a	$\Phi_{ACE\ /adj}$			296	**31.9**	**515.21**	81.4		**13.57**	**39.04**		453.2	469.7
DLR	Φ_{ACE}			296	**31.9**	**515.21**	81.4		**13.95**	**41.14**			
BO96	$\Phi_{ClimaxNM}$					**501.13**			**17.1**	**46.78**			
	1/22/1998	8.82	51.6	296	50.3	493	94.6	92.4	14.9	52.9			
BO11				**296**	**31.9**		**81.4**		**15.39**	**43.86**	**Al 7" sphere**	**503.5**	**463.3**
BO10_a	$\Phi_{ACE/adj}$			296	**31.9**	**515.21**	81.4		**14.27**	**38.8**		453.2	469.7
DLR	Φ_{ACE}			296	**31.9**	**515.21**	81.4		**14.66**	**40.67**			
BO96	$\Phi_{ClimaxNM}$					**501.13**			**18.08**	**47.31**			
	1/22/1998	8.82	51.6	296	50.3	493	94.6	92.4	17.1	49.2			
BO11				**296**	**31.9**		**81.4**		**16.04**	**43.12**	**Al 9" sphere**	**503.5**	**463.3**
BO10_a	$\Phi_{ACE/adj}$			296	**31.9**	**515.21**	81.4		**14.9**	**38.62**		453.2	469.7
DLR	Φ_{ACE}			296	**31.9**	**515.21**	81.4		**15.31**	**40.34**			
BO96	$\Phi_{ClimaxNM}$					**501.13**			**18.96**	**47.84**			

The Mars Science Laboratory "Curiosity" Rover Science Payload

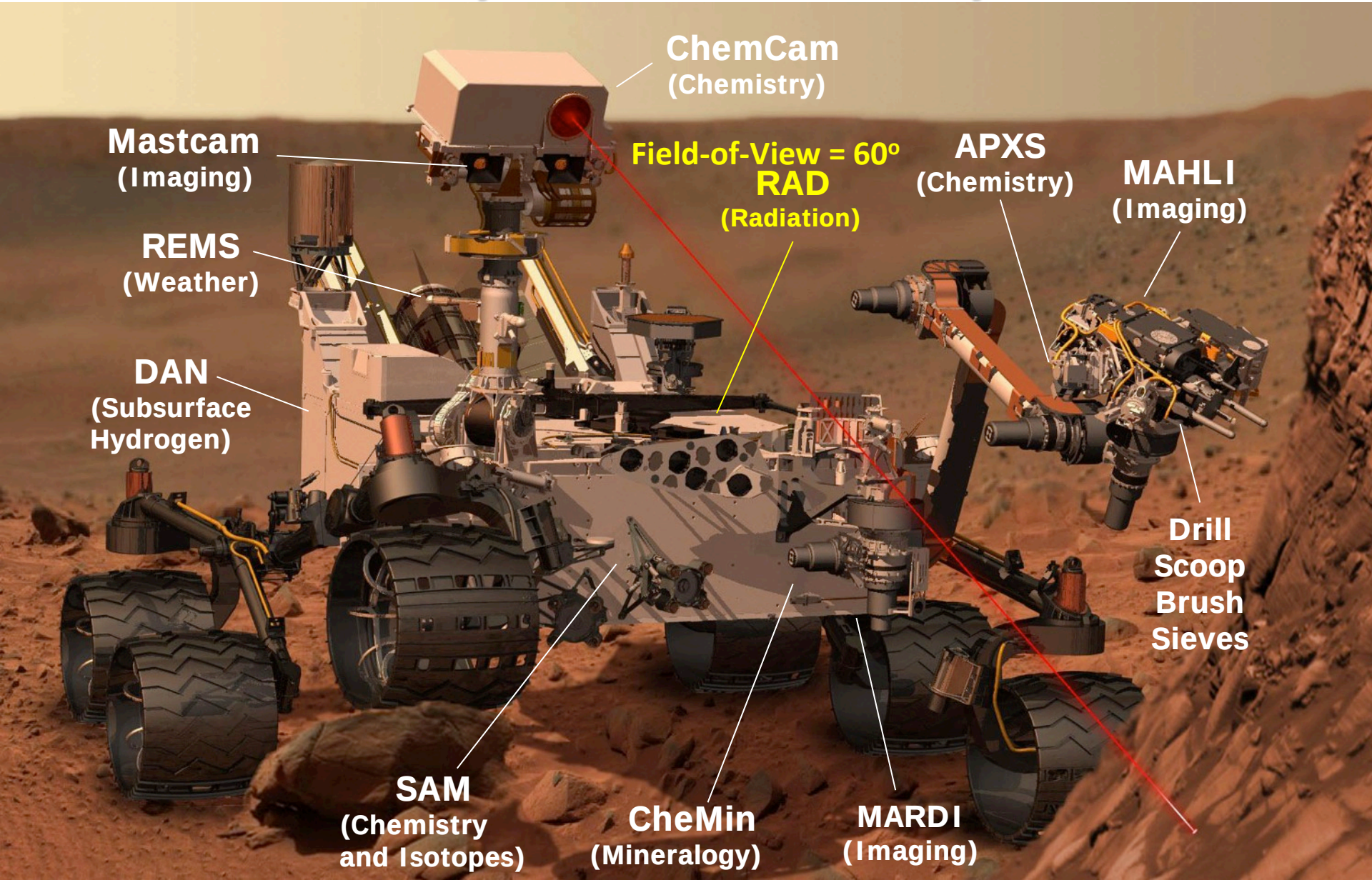

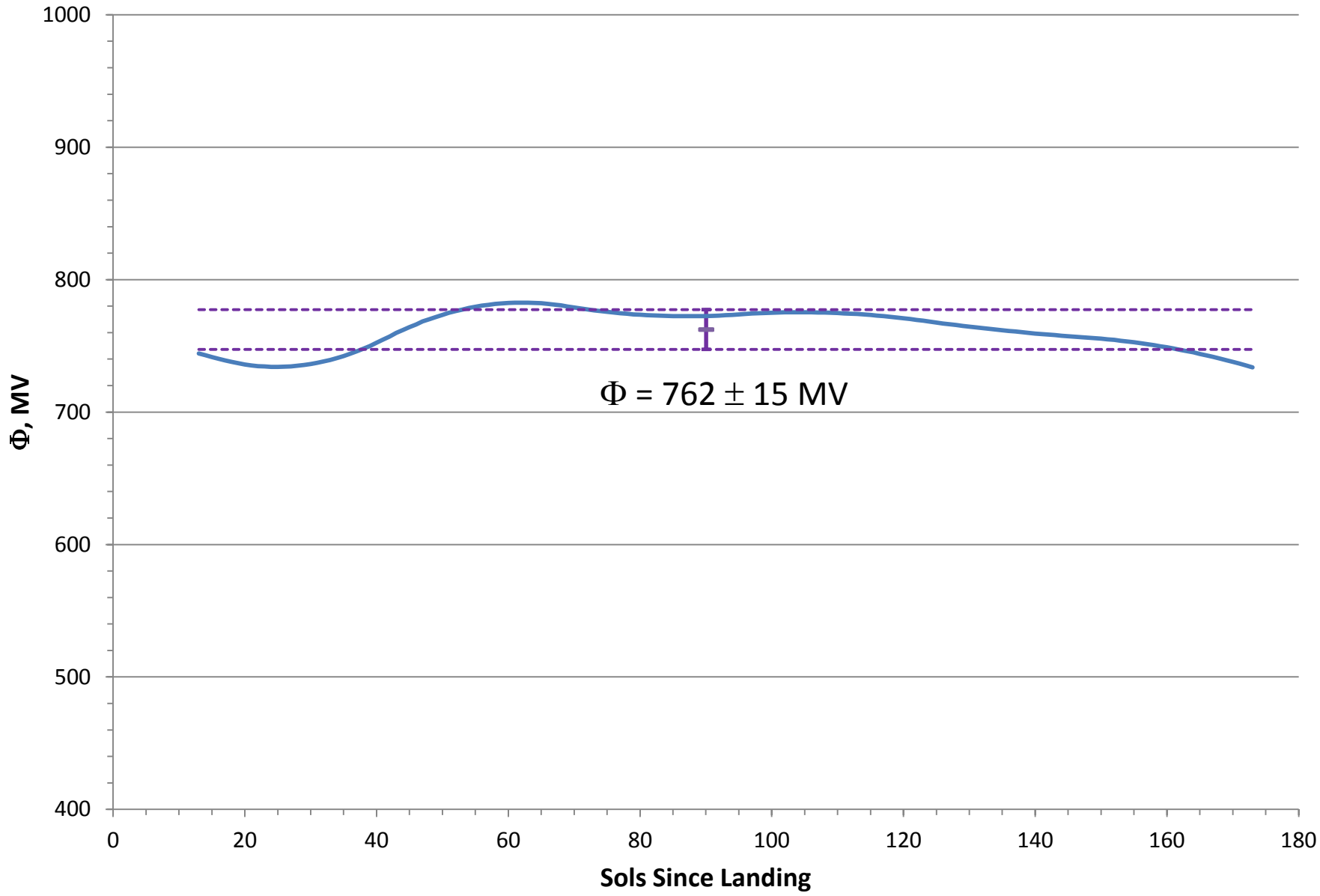
Solar Modulation Parameter using BO11 GCR Model for sols 13 to 173
1000
900
800
700
600
500
400
Φ, MV
Φ = 762 ± 15 MV
0
20
40
60
80
100
120
140
160
180
Sols Since Landing

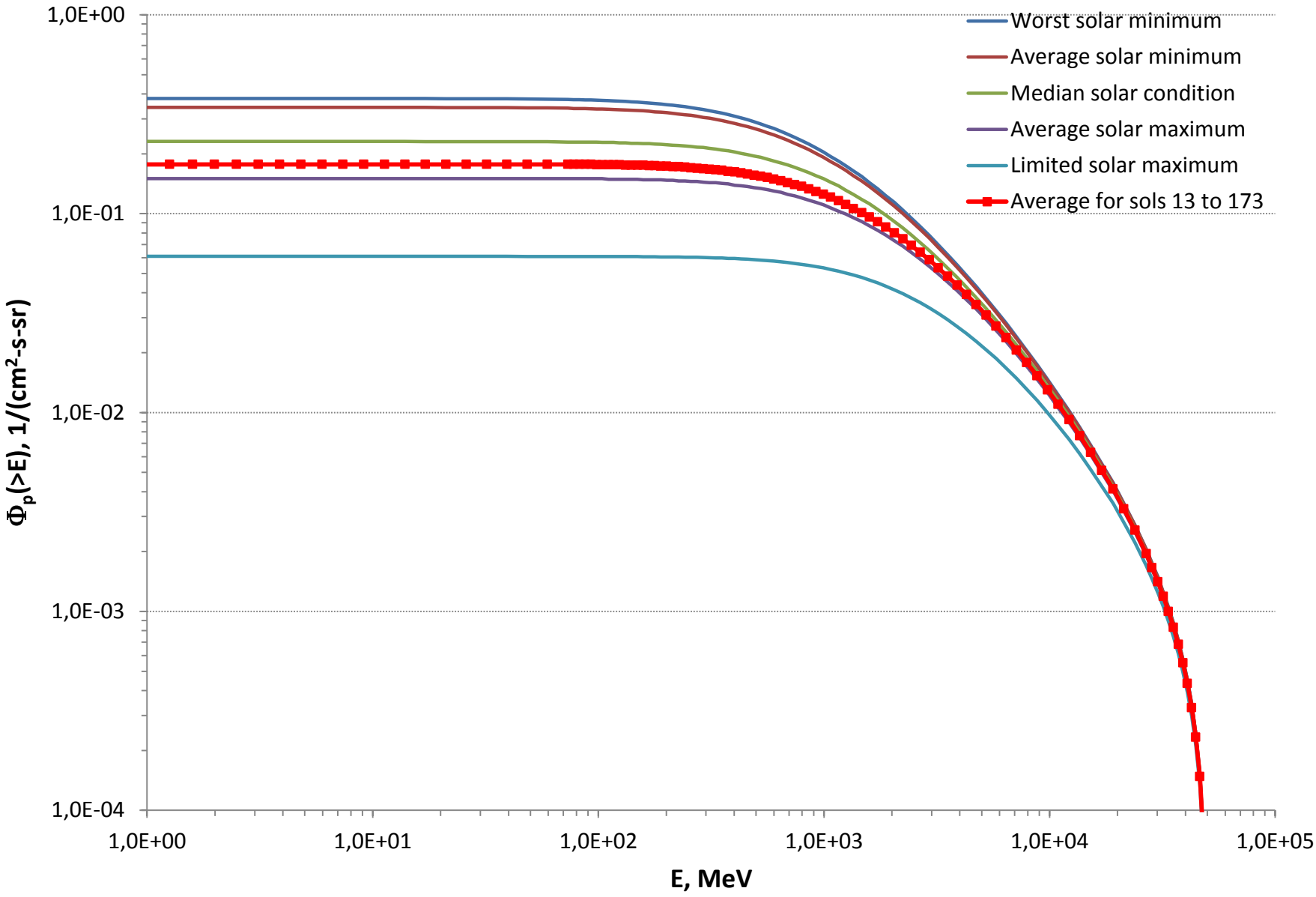
Integral Proton Flux in Interplanetary Space for Various Solar Condition
1,0E+00
1,0E-01
1,0E-02
1,0E-03
1,0E-04
Φ_p(>E), 1/(cm^2-s-sr)
1,0E+00
1,0E+01
1,0E+02
1,0E+03
1,0E+04
1,0E+05
E, MeV
Worst solar minimum
Average solar minimum
Median solar condition
Average solar maximum
Limited solar maximum
Average for sols 13 to 173

Daily Average Column Depth Measurements by MSL/Rover Environmental Monitoring Station

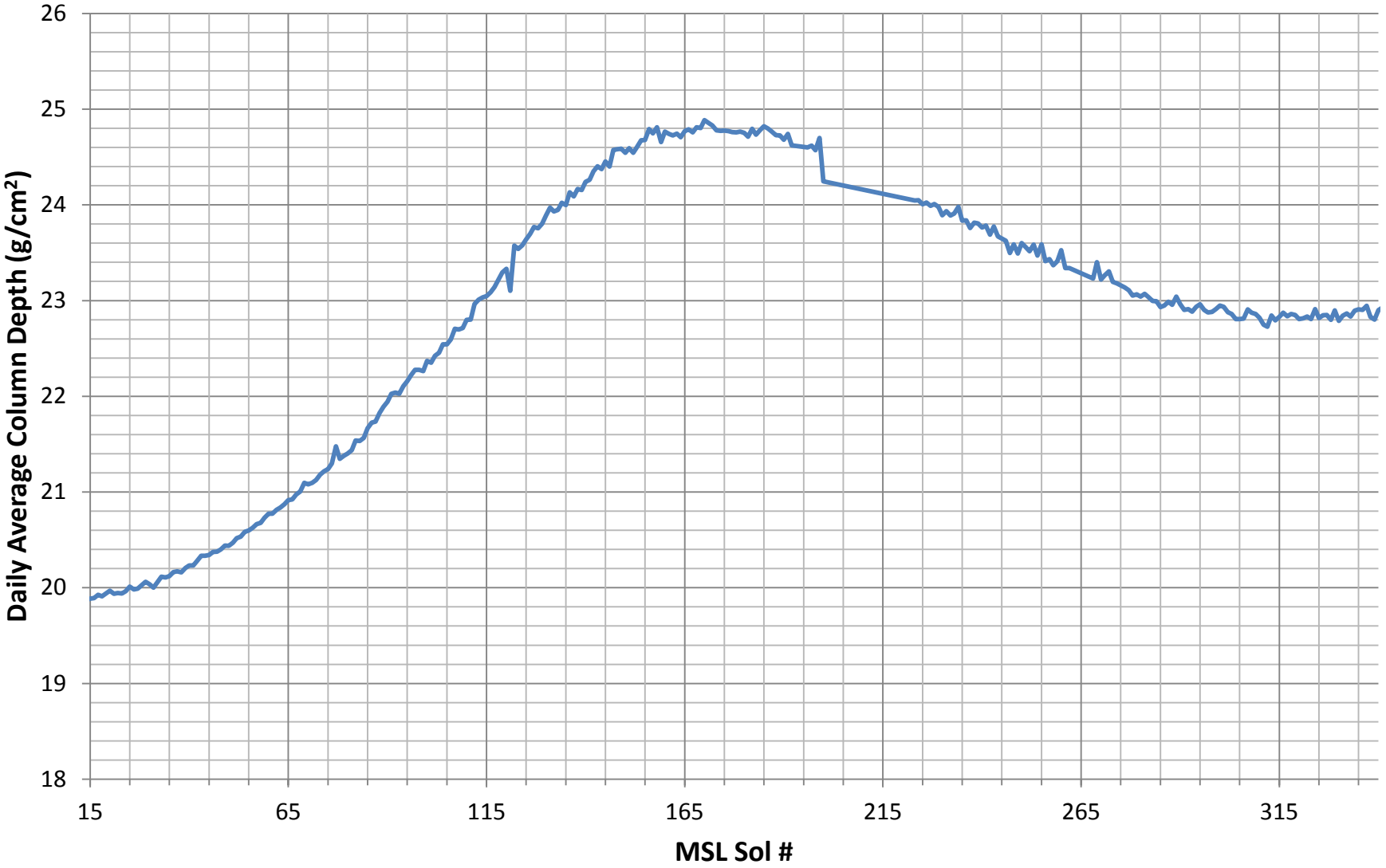

Gómez-Elvira, J., et al. (2012), REMS: The environmental sensor suite for the Mars Science Laboratory rover, Space Sci. Rev., 170(1–4), 583–640.

Spherical Distribution of CO_2 Thickness along the Slant Path at *Gale* Crater on Mars

$$s(z,\theta) = \sqrt{(R+h)^2\cos^2(\theta) + [2R(z-h) + z^2 - h^2]} - (R+h)\cos(\theta)$$

s: the distance along the slant path, g/cm^2
z: the vertical height of the Mars atmosphere (at Gale crater, g/cm^2)
θ: zenith angle
R: the radius of Mars, g/cm^2
h: the elevation above the Gale crater, km

MSL/RAD Sensor Head (RSH)

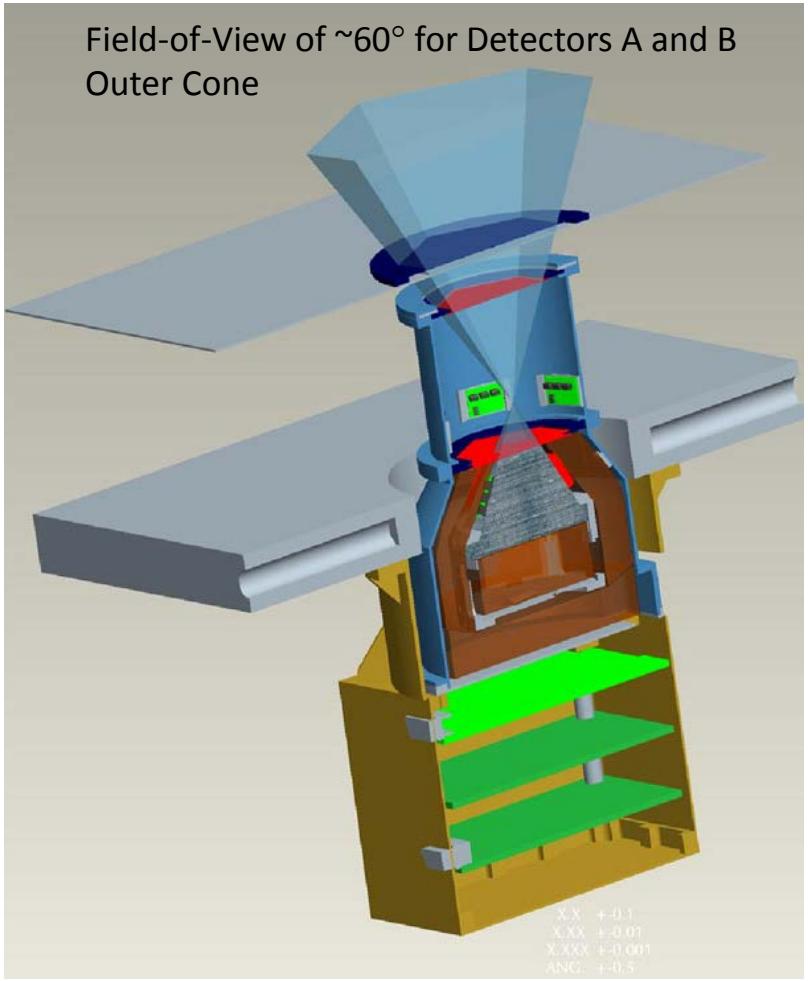

Thickness for RSH

Detector	Material	$R_{Mat}(p_{50\ MeV})$, g/cm²	ρ, g/cm³	t_{Mat}, g/cm²	$t_{Al\text{-}Eq}$, g/cm²
SSD A	Si	2.822	2.33	negligible	
SSD B	Si	2.822	2.33	negligible	
SSD C	Si	2.822	2.33	negligible	
D	CsI	4.34	4.51	12.6	8.5
E	Scintillating plastic	2.063	0.95	1.8	2.5
F				1.1	1.6

RAD Geometry Factors

Field of view	G_F (cm² sr)	Segment
(A1+A2)·B·C·D	0.90	A1 inner + A2 outer cone combined
A2·B·C·D	0.17	A2 inner cone
E	209	$G = \pi A$ for isotropic radiation

Hassler, D. M., et al. (2012), The Radiation Assessment Detector (RAD) investigation, Space Sci. Rev., 170(1–4), 503–558.

Schematic Diagram and Dimension of RAD Instrument for Ray Tracing at the Dose Point of *E* Detector

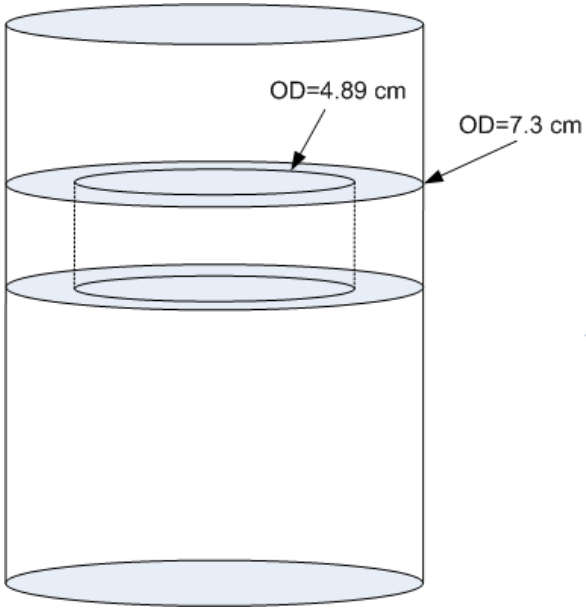

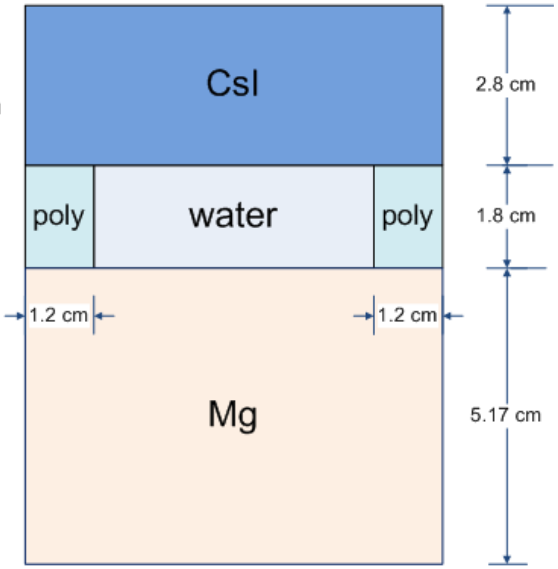

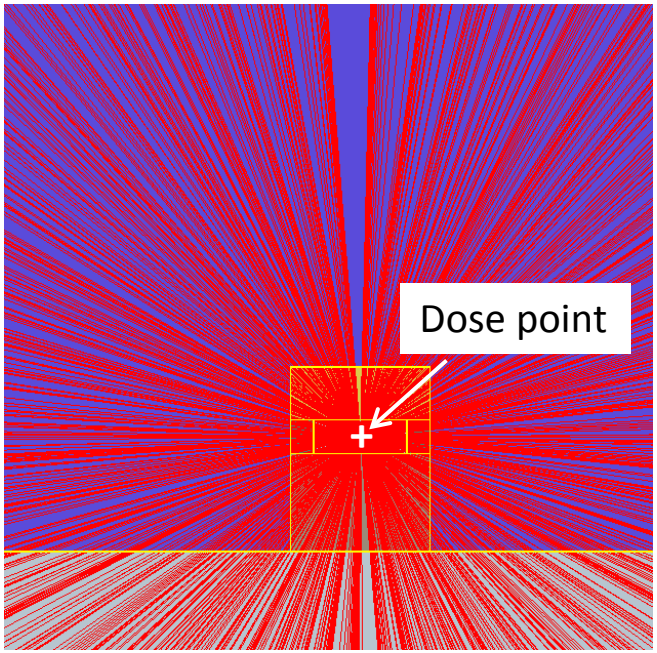

Kim, M.-H. Y., et al. (2014), Comparison of Martian surface ionizing radiation measurements from MSL-RAD with Badhwar-O'Neill 2011/HZETRN model calculations, *J. Geophysical Research – Planets*, 119(6):1311-1321, doi:10.1002/2013JE004549.

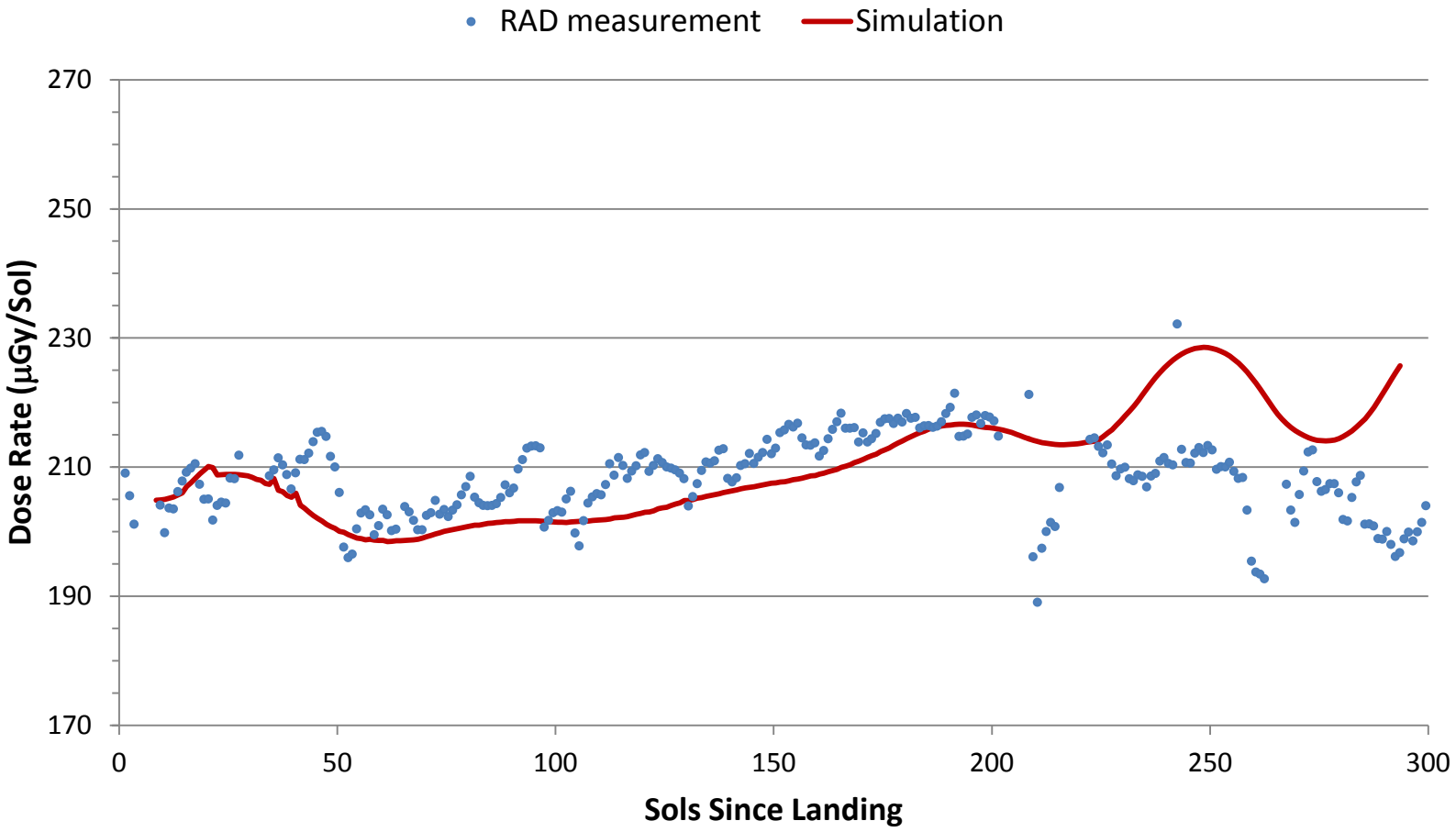

Kim, M.-H. Y., et al. (2014), Comparison of Martian surface ionizing radiation measurements from MSL-RAD with Badhwar-O'Neill 2011/HZETRN model calculations, *J. Geophysical Research – Planets*, 119(6):1311-1321, doi:10.1002/2013JE004549.

Validation Metric

Error Analysis with the Measurement Uncertainty

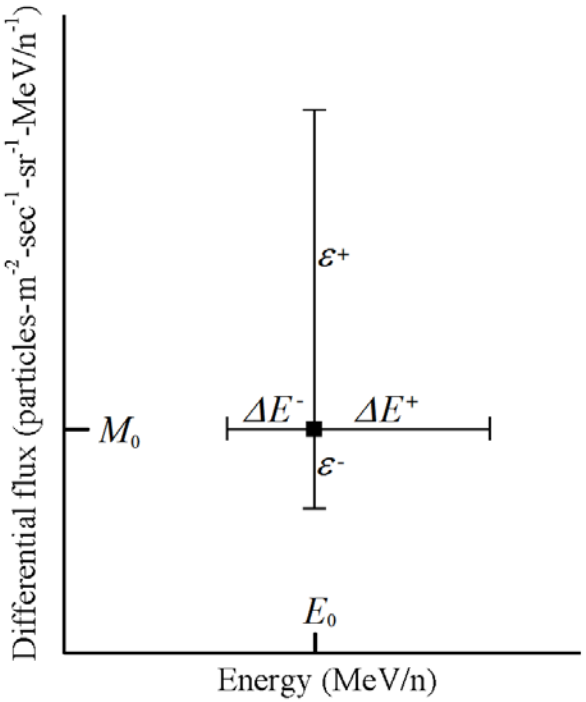

Typical Measurement for GCR Flux

$$R_D = \frac{F - M_0}{M_0}$$

Relative difference using nominal measurement

$$U_{upper} = \frac{F - [M_0 - \varepsilon^-]}{M_0 - \varepsilon^-}$$

Uncertainty relative to lower error bar

$$U_{lower} = \frac{F - [M_0 + \varepsilon^+]}{M_0 + \varepsilon^+}$$

Uncertainty relative to upper error bar

- Sentz and Ferson, Reliability Engineering and System Safety, **96**: 1126-1136 (2011).
- Ferson et al., Sandia Report SAND2007-0939 (2007).

Measurement Database

Name	Flight	Time	Ions (Z)	Energy (GeV/n)	Data pts.	Median Error
ACE/CRIS	Satellite	1998-present	5-28	0.05-0.5	8288	10%
AMS	STS-91	1998	1,2	0.1-200	58	11%
ATIC-2	Balloon	2002	1,2,6,8..,26	$4.6\text{-}10^3$	55	33%
BESS	Balloon	1997-2000,2002	1,2	0.2-22	300	12%
CAPRICE	Balloon	1994, 1998	1,2	0.15-350	93	6%
CREAM-II	Balloon	2005	6-8,10,12,14,26	$18\text{-}10^3$	42	25%
HEAO-3	SatelliteB	1979	4-28	0.62-35	331	9%
IMAX	alloon	1992	1,2	0.18-208	56	18%
IMP-8	Balloon	1974	6,8,10,12,14	0.05-1	53	28%
LEAP	Balloon	1987	1,2	0.18-80	41	30%
MASS	Balloon	1991	1,2	1.6-100	41	10%
PAMELA	Satellite	2006-2009	1,2	$0.08\text{-}10^3$	472	11%
TRACER	Balloon	2003	8,10,12..20,26	$0.8\text{-}10^3$	55	11%
Lezniak	Balloon	1974	4-14,16,20,26	0.35-52	131	12%
Minagawa	Balloon	1975	26,28	1.3-10	16	19%
Muller	STS-51	1985	6,8,10,12,14	$50\text{-}10^3$	16	27%
Simon	Balloon	1976	5-8	$2.5\text{-}10^3$	46	33%

10,101 measurement data points

Model Comparison by Energy Group

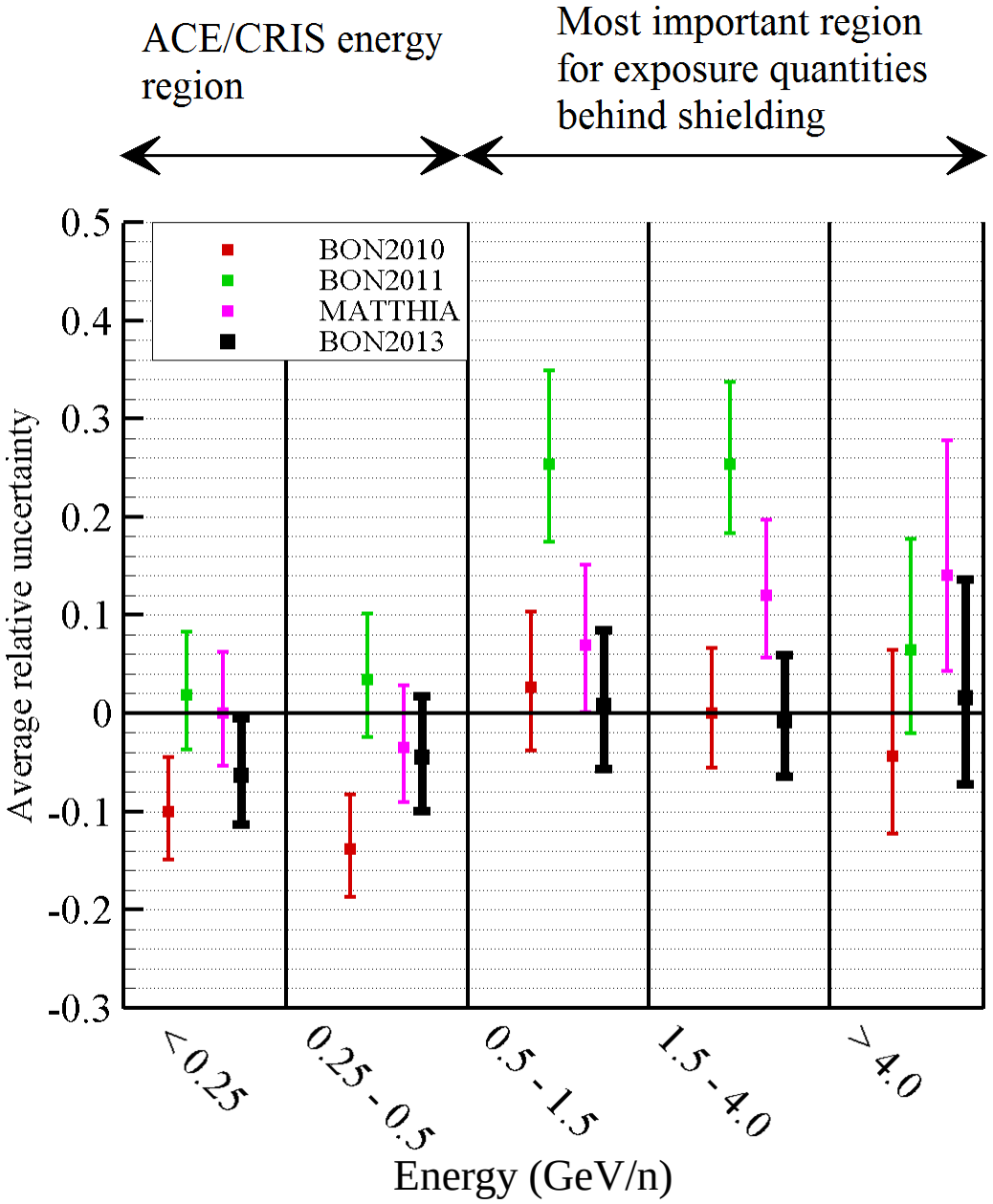

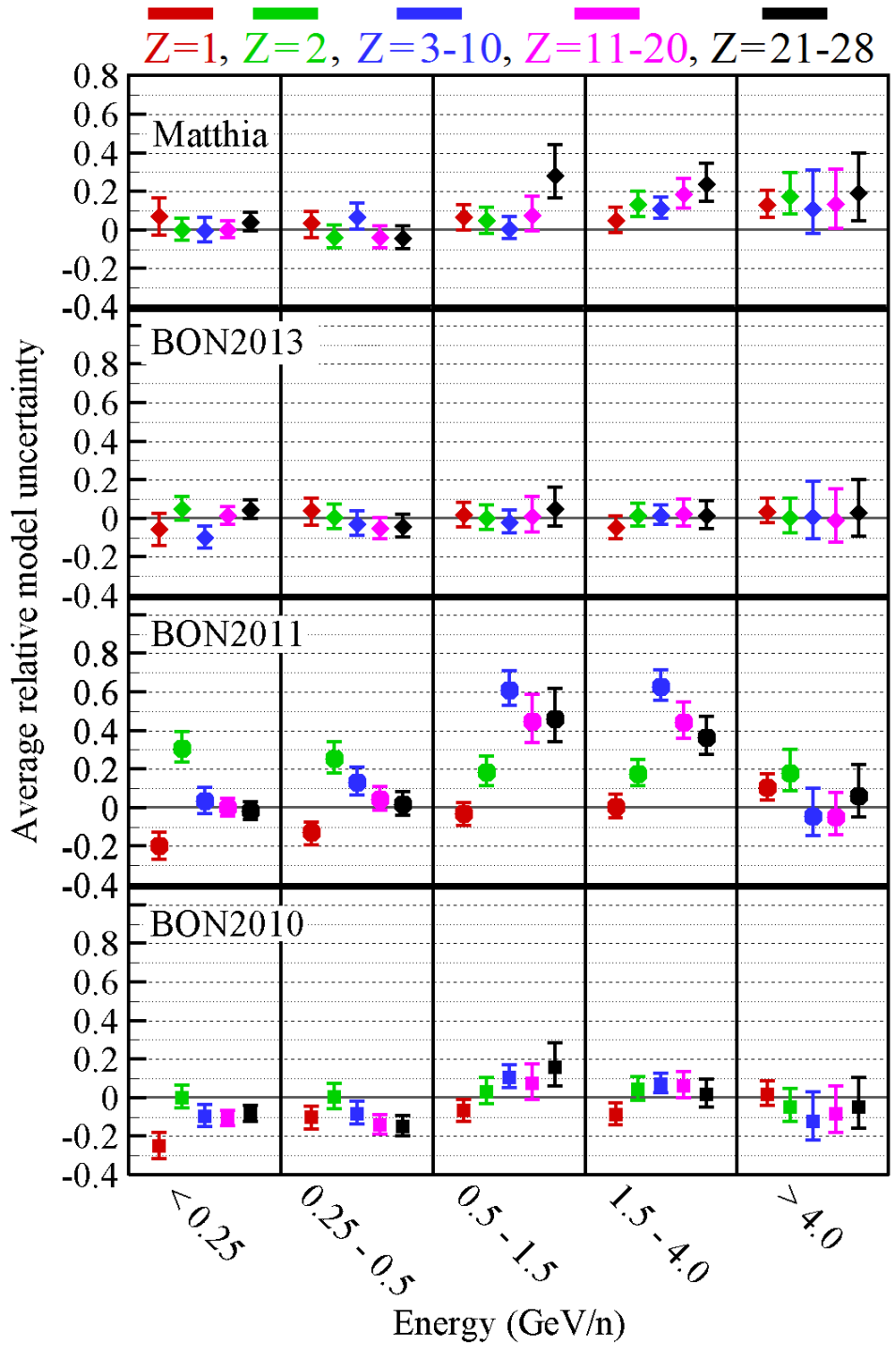

Average over All Measurements

Model	R_D	$[U_{lower}, U_{upper}]$
BO2010	-10%	[-15%, -3%]
BO2011	4%	[-2%, 11%]
BO2013	-5%	[-10%, 2%]
Matthia	1%	[-5%, 8%]

Conclusions

- BO11 model agrees reasonably well with measurements and fundamentally sounds for the application to space radiation risk analysis.
- By advantage of using sunspot numbers for BO11 model, retrospective analyses were made for the past ISS missions.
- The BO11 model was applied to calculate the absorbed doses of RAD instrument at *Gale* crater for ~300 sols since the landing on August 6, 2012.
  - ✓ The simulated total dose rates using BO11/HZETRN agree on average to within ±15% with the RAD measurements.
  - ✓ The simulation shows in relatively good agreement with the RAD data for the first 200 sols, because BO11 has emphasized for the last 24-solar minima.
  - ✓ The simulation is resulted in less agreement near the solar maximum of solar cycle 24, due to subtleties in the changing heliospheric conditions.
- By the error analysis, the BO model is optimized in reducing overall uncertainties.
  - ✓ The resultant BO model corrects the fit at solar maxima as well as being accurate at solar minima.
  - ✓ It will be implemented for the space radiation risk assessment and probabilistic radiation risks can be assessed to support mission design and operational planning.